EFFECTS OF COARSE-GRAINED TARGETS ON CRATER MORPHOLOGY. H. C. M. Susorney[1], R. T. Daly[2], O. S. Barnouin[2,3], A. M. Stickle[2], C. M. Ernst[2], D. A. Crawford[4], and M. J. Cintala[5] [1]2020 – 2207 Main Mall, University of British Columbia, Vancouver, BC Canada V6T 1Z4 (hsusorney@eoas.ubc.ca), [2]Johns Hopkins University Applied Physics Laboratory, Laurel, MD 20723, USA, [3]High Energy Material Institute Johns Hopkins University, Baltimore, MD 21218, USA, [4]Sandia National Laboratories, Albuquerque, NM 87185, USA, and [5]NASA Johnson Space Center, Houston TX 77058, USA.

Introduction: Craters formed in coarse-grained targets can have unusual morphologies that probably result from the complex interactions of shock waves with the many interfaces and free surfaces in the target [e.g., 1,2]. These effects are likely important for asteroids, which often have surfaces covered in boulders [3,4] and where self-armoring may reduce the efficiency of crater formation [5].

Recent experimental work on coarse-grained targets has focused on the ratio of projectile diameter to target grain size [6,7,8]. The results have been mixed, with [6] finding that, at low velocities, this ratio has a significant effect but [8] finding almost no effect at higher speeds. Experiments by [7] bridged this gap by showing that another factor, the ratio between the impactor kinetic energy and the disruption energy for a target grain, is needed to explain the outcomes.

In this study, we use numerical models to investigate how coarse-grained targets affect transient crater morphology, emphasizing in particular the ratio between the width of the shock, *w,* and the diameter of the target grains, *d* (Fig. 1), while varying target strength to constrain the effects of disruption energy.

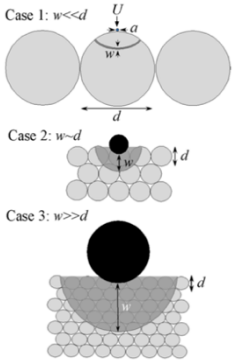

Figure 1. Schematic illustration of the relationship between shock width, *w*, and target grain size, *d*. The projectile (black) has diameter, *a,* and impacts with a velocity, *U*. In Case 1 the shock width (dark gray) is far narrower than the diameter of the grains. In Case 2 the shock width and grain size are comparable. In Case 3 the shock width is much wider than the grain size.

Methodology: The multi-material, multi-dimensional, Eulerian shock physics code CTH [9] was used to model impacts into targets of various "grain" sizes. We modeled targets using 2d-cylindrical (2DC) and 2d-rectangular (2DR) geometries. In 2DC, the grains are toroids, whereas in 2DR, the grains are infinite rods. The target grain (i.e., toroids or rods) interactions were modeled in two ways. In the first case, they were not permitted to slide past one another but could merge. In the second, the grains were allowed to slide past one another using the SLIDE option in CTH, which sets the shearing velocity components to zero in mixed cells. We used the SESAME equation of state [10] for basalt for both the projectile and target. We varied impact speed and target grain size in order to explore a broad range of *w/d*. The projectile diameter was fixed at 1 cm. We ran models until crater growth ceased and measured the ratio of transient crater depth to diameter in each simulation. A suite of fixed tracers recorded the pressure and temperature field.

Simulations were done using two constitutive models: linearly elastic, perfectly plastic and the "Geological Yield" Surface. The elastic, perfectly plastic strength model allows us to vary target strength easily, although it does not accurately represent the behavior of basalt. The Geological Yield Surface better represents the constitutive response of basalt by adding pressure dependence to the yield surface.

Results: Figure 2 shows preliminary results using the linearly elastic, perfectly plastic strength model (with fixed target strength of 100 MPa) and grains which were not allowed to slide past each other. Figure 2 shows pressure fields from models of Case 1, 2, and 3 impacts (Fig 1), as well as a reference case: an impact into a half-space.

The shock wave travels fastest in the half space; peak pressures are also highest in this model. In Case 1, the shock wave travels at similar speeds to the wave in the half space, but peak pressures were reduced by 4%. The initial shock wave travels slowest in the Case 2 impact. The Case 2 pressure field is further attenuated compared to the half-space reference case, with a 63% reduction in peak pressure at a tracer 4 cm beneath the impact point. Moreover, the propagating pressure wave diffuses and loses its hemispherical shape with time (Fig 2d). In Case 3, the initial shock wave travels faster than in Case 2 and maintains its hemispherical shape, but with peak pressure reduced by 66% compared to the half-space at the same tracer 4 cm beneath the impact point.

The three cases for elastic, perfectly plastic yielded different transient depth/diameter ratios. The simulations for Cases 2 and 3 impacts had the largest depth/diameter ratios (d/D = 0.64 and 0.65, respectively). The depth/diameter ratio in Cases 2 and 3 exceeded that in

the half space simulation (d/D = 0.60). Case 1 led to the smallest depth/diameter ratio (d/D = 0.46), where we believe boundary effects dominated crater growth. Cratering efficiency (π_v, the ratio of volume displaced to the volume of the projectile) also varied. The half space had a cratering efficiency of 42, while Cases 1, 2, and 3 have cratering efficiencies of 43, 36, and 36, respectively.

Discussion: Interactions between the propagating shock wave and the boundaries of the grains likely account for the differences between Case 1, 2, and 3. These interactions affect the rates of shock propagation and attenuation, as well as peak pressures and the shape of the advancing pressure wave front.

In Case 1 impacts, the first target grain hit by the impactor acts much like a half space at early times. Later, interactions among rarefaction waves off the first target grain's free surfaces cause additional attenuation. In Case 2 impacts, the difficulty of transferring the shock from one grain to the next, combined with the multitude of rarefaction waves off the large number of free surfaces, act to slow shock propagation and reduce peak pressures. The shock wave no longer "sees" individual grains in case 3 impacts, but rather propagates through what is effectively a porous material. Consequently, pore-space collapse (irreversible pressure-volume work) consumes energy and enhances attenuation. The decrease in cratering efficiency seen for Case 2 and 3 impacts relative to their Case 1 impacts and the half space counterparts likely also reflects the role of energy dissipation associated with pore-space collapse.

Conclusion: When their target yield strengths are fairly low, coarse-grained targets show differences in shock propagation, peak pressure, and geometry compared to impacts into a half space. Changing the ratio between the width of the shock and the diameter of the target grains affects both transient crater depth/diameter ratio and cratering efficiency. These changes likely arise from (a) the small contact areas between grains, which limits shock propagation and (b) the large number of curved free surfaces in the problem, which introduce additional, complex geometric effects.

Comparisons between the half-space scenario and Cases 2 and 3 further illustrate this point. Following passage of the shock, rarefaction waves off of free surfaces establish the cratering flow field. In the half-space impact. The flat surface of the half space, on the other hand, is the only relevant free surface affecting crater growth. However, Case 2 and 3 impacts generate rarefaction waves off the boundaries of each grain, which can create stark differences in the cratering flow field, in addition to affecting shock attenuation and peak pressure. We expect stronger targets with more complex constitutive properties will reveal different behaviors, which could explain why some laboratory experiments show high cratering efficiency despite having a *w/d* ratio ~1 [11].

References: [1] Cintala M. J. et al. (1999) *Meteoritics & Planet. Sci.* 34, 605–623. [2] Jutzi M. (2014) *Icarus* 229, 247–253. [3] Ververka J. et al. (2000) *Science* 289, 2088–2097. [4] Fujiwara A. (2006) *Science* 312, 1330–1334. [5] Hirata N. et al., (2009) *Icarus* 200, 486–502. [6] Güttler C. et al. (2012) *Icarus* 220, 1040–149. [7] Tatsumi and Sugita (2017) *Icarus* in press, doi: 10.1016/j.icarus.2017.09.004. [8] Holsapple, K. A. and Housen, K. R. (2014) *LPS 45* abstract 2538. [9] McGlaun, J M., et al. (1990) *Int. J. Impact Eng.* 10, 351–360. [10] Kerley G. I. (1999) *Kerley Publishing Services Report* KPS99-4. [11] Barnouin et al. *Icarus,* submitted.

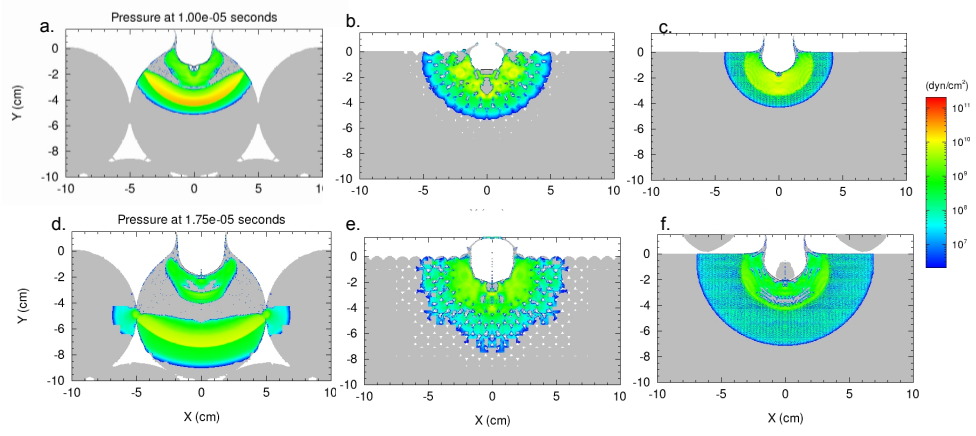

Figure 2. Pressure field for Case 1 (a, d), Case 2 (b, e), and Case 3 (c, f) for 10 μs and 17.5 μs after impact. The gray and white regions represent the target and voids, respectively. The targets and projectiles are modeled as basalt, using the SESAME equation of state and a simple elastic, perfectly plastic strength model.